Placenta 43 (2016) 90–97

Contents lists available at ScienceDirect

Placenta

journal homepage: www.elsevier.com/locate/placenta

A longitudinal study of placental perfusion using dynamic contrast enhanced magnetic resonance imaging in murine pregnancy☆

Brijesh Kumar Yadav [a, b], Jaladhar Neelavalli [a, b, *], Uday Krishnamurthy [a, b], Gabor Szalai [c], Yimin Shen [a], Nihar R. Nayak [d], Tinnakorn Chaiworapongsa [c, d], Edgar Hernandez-Andrade [c, d], Nandor Gabor Than [c, d, e], E. Mark Haacke [a, b], Roberto Romero [c, f, g, h]

[a] Department of Radiology, Wayne State University School of Medicine, Detroit, MI, USA
[b] Department of Biomedical Engineering, Wayne State University College of Engineering, Detroit, MI, USA
[c] Perinatology Research Branch, NICHD/NIH/DHHS, Bethesda, MD, and Detroit, MI, USA
[d] Department of Obstetrics and Gynecology, Wayne State University School of Medicine, Detroit, MI, USA
[e] Lendulet Reproduction Research Group, Institute of Enzymology, Research Centre for Natural Sciences, Hungarian Academy of Sciences, Budapest, Hungary
[f] Department of Obstetrics and Gynecology, University of Michigan, Ann Arbor, MI, USA
[g] Department of Epidemiology and Biostatistics, Michigan State University, East Lansing, MI, USA
[h] Center for Molecular Medicine and Genetics, Wayne State University, Detroit, MI, USA

ARTICLE INFO

Article history:
Received 25 June 2015
Received in revised form
18 December 2015
Accepted 31 December 2015

Keywords:
Labyrinth zone
Junctional zone
Contrast enhanced
Central canal
Mice

ABSTRACT

Introduction: To evaluate changes in placental perfusion with advancing gestation in normal murine pregnancy using dynamic contrast enhanced magnetic resonance imaging (DCE-MRI).
Methods: Seven timed-pregnant CD-1 mice underwent DCE-MRI scanning longitudinally on gestational days (GD) 13, 15 and 17. Placentas were segmented into high (HPZ) and low perfusion zones (LPZ) using tissue similarity mapping. Blood perfusion of the respective regions and the whole placenta was quantified using the steepest slope method. The diameter of the maternal central canal (CC) was also measured.
Results: An increase in perfusion was observed between GD13 and GD17 in the overall placenta ($p = 0.04$) and in the HPZ ($p = 0.02$). Although perfusion in the LPZ showed a slight increasing trend, it was not significant ($p = 0.07$). Perfusion, in units of ml/min/100 ml, in the overall placenta and the HPZ was respectively 61.2 ± 31.2 and 106.2 ± 56.3 at GD13 ($n = 19$ placentas); 90.3 ± 43.7 and 139 ± 55.4 at GD15 ($n = 20$); and 104.9 ± 76.1 and 172.2 ± 85.6 at GD17 ($n = 14$). The size of the CC increased with advancing gestation ($p < 0.05$).
Discussion: Using longitudinal DCE-MRI, the gestational age-dependent perfusion change in the normal murine placenta and in its regional compartments was quantified. In mid and late gestations, placental constituent regions differ significantly in their perfusion rates. The CC diameter also showed increase with advancing gestation, which may be playing an important role toward the gestational age-dependent increase in placental perfusion.

1. Introduction

The placenta plays a crucial role in providing adequate nourishment to the developing fetus. It meets the growing metabolic demands of the fetus through appropriate gestation-dependent structural, morphological and functional changes [1]. Increases of the overall size and vascular remodeling, including changes of vessel length, diameter and vessel density per unit volume, in both maternal and fetal circulation compartments are known to occur

☆ Part of the data reported in this paper was presented as a scientific oral presentation at the *"Annual Meeting of the International Society of Magnetic Resonance in Medicine"* in Toronto, Ontario, Canada, May 30-July 05, 2015. The work won the "*Summa cum laude*" merit award.

* Corresponding author. Department of Radiology, Wayne State University School of Medicine, 4201 St. Antoine, Detroit, MI 48201, USA.
E-mail address: jneelava@med.wayne.edu (J. Neelavalli).

http://dx.doi.org/10.1016/j.placenta.2015.12.019
0143-4004/

[2–7]. Decrease in vascular resistance is thought to help the efficiency of placental and fetal perfusion [6,8]. Abnormal remodeling of spiral arteries in the placental bed leading to reduced blood supply to the placenta is one of the features observed in obstetric conditions such as preeclampsia and fetal growth restriction (FGR) [9–12]. Indeed, placental ischemia has been implicated as a common factor in serious pregnancy complications — placental abruption, FGR and preeclampsia [13]. Therefore, evaluating placental functional status has become important in obstetric evaluation [14,15], and placental blood perfusion is one of the central indicators of placental function.

Despite its importance as a marker of placental function, our ability to non-invasively measure regional placental perfusion in humans is limited. Dynamic contrast enhanced magnetic resonance imaging (DCE-MRI) is a standard technique that uses an exogenous contrast agent (often gadolinium chelate based) for quantifying organ perfusion in ml/min per unit weight or volume of the tissue [16]. Use of MRI contrast agents, however, is contraindicated during pregnancy in humans [17]. In this context, murine models of pregnancy have become an important means for studying and understanding placental development and etiology of various human obstetrical conditions due to the anatomical, functional and cellular similarities between the two [18–23]. Use of contrast enhanced MRI methods in animal models has helped to advance our understanding of the pathophysiology of various conditions [24–26].

DCE-MRI is a powerful method which has been used previously for evaluating placental perfusion in mice [19,27–29]. By this technique, an exogenous MRI contrast agent is injected into the blood stream and, as it traverses the organ of interest, the change in the MRI signal can be observed by taking a series of snapshots of the organ. The temporal contrast-uptake measured from the image time-series provides qualitative and quantitative information about tissue blood perfusion. Previous DCE-MRI studies in mice have shown qualitative differences in placental perfusion between normal and disease conditions [18,30,31] at a given gestation. Although anticipated [32], normal gestational age-dependent change in murine placental perfusion, however, has not been quantified before. While uterine and umbilical flow changes have been characterized across gestation in murine pregnancy [33,34], similar studies measuring regional placental perfusion are scant [35]. Moreover, the placenta is a heterogeneous structure with different constituent regions performing different functional roles. During advancing gestation, the adaptation/changes occurring in these regions may also be distinct. Hence, to understand the normal placental hemodynamic adaptation, it is important to evaluate the regional changes in perfusion as a function of gestational age. In this study, we evaluated the longitudinal changes in murine placental perfusion in mid and late gestation using quantitative analysis of DCE-MRI. Specifically, we evaluated perfusion in the two constituent regions of the murine placenta, the high perfusion zone (HPZ) on the fetal side of the placenta and the low perfusion zone (LPZ) on the maternal side of the placenta, on gestational days (GD) 13, 15 and 17. In previous works, these high and low perfusion zones have been identified in murine placenta using contrast enhanced ultrasound or MRI, based on their characteristic fast or slow uptake of contrast agents [29,36,37]. The HPZ roughly corresponds to the base of the labyrinth zone supplied by the maternal central canal (CC) and the LPZ roughly to the junctional zone. The CC in murine placentas has a functional similarity with that of the spiral arteries in the human placenta in that they both act as important conduits to feed the maternal blood into the region where maternal-fetal metabolic exchange occurs. We also measured the diameter of the maternal CC on the three GDs.

2. Materials and methods

2.1. Animal care and handling

The study protocol was approved by the Institutional Animal Care and Use Committee (IACUC) at Wayne State University (Detroit, MI, USA). Animal care and handling followed the standards set forth by the National Research Council of the National Academies [38]. Timed-pregnant CD-1 mice (n = 7) were obtained from Charles River Laboratories (Wilmington, MA, USA). Pregnancy was confirmed by manual examination on GD12. Mice were kept separately in filter-top rodent cages and fed with *ad libitum* water and food. A regular 12:12 h dark–light cycle and constant temperature (24±1 °C) and humidity (50 ± 5%) were maintained in the animal room, and mice were monitored for food and water intake, vital signs, behavior and activity.

2.2. Magnetic resonance imaging

All MR studies were performed on a dedicated small animal MR scanner 7.0 T, 30 cm bore superconducting magnet (ClinScan, Bruker, Karlsruhe, Germany) interfaced with a Siemens Syngo console. A standard circularly polarized body coil insert was used for imaging. Prior to data acquisition, anesthesia was induced by isoflurane mixed with air to sedate the animals (4% v/v via an induction chamber and then 1.5–2% v/v for maintenance of sedation). Mice were kept under anesthesia throughout the data acquisition. The contrast agent bolus injection was carried out manually over 22 s starting at imaging time point 9. The bolus consisted of 0.5 M gadolinium-based contrast agent, Magnevist (Gadopentetate dimeglumine – Gd-DTPA), diluted 1:10 with saline to 0.25 ml (i.e., 0.0125 mmol of Gd-DTPA), which was injected through a catheter placed in the tail vein. The gadolinium dose was approximately 0.3 mmol/kg for a 42 g pregnant mouse.

The DCE-MRI scan consisted of an initial acquisition for the estimation of baseline tissue longitudinal relaxation time (T_1) followed by the dynamic series acquisition during contrast injection and uptake. A multi-slice two-dimensional (2D) spoiled gradient echo sequence was used for DCE-MRI data acquisition. Imaging parameters were: echo time (TE) = 2.02 ms, repetition time (TR) = 43 ms, resolution = 0.27 × 0.27 × 1.5 mm^3, slice gap = 2 mm, bandwidth = 260 Hz/pixel, and matrix size = 128 × 128. For the estimation of baseline T_1, data was acquired using this sequence with three different flip angles (FA), 5°, 13° and 30° — each with the number of averages (navg) = 8 for high signal-to-noise ratio (SNR). For acquisition during contrast injection and uptake, the same sequence with navg = 1 and FA = 30° was used. A total of 7 slices was acquired with a temporal resolution of 5.5 s, and the data was acquired for 150 time points. During dynamic data acquisition, the contrast agent was injected manually after acquiring 9 volumes which provided a baseline ($S(t{=}0)$) relative to which the contrast-uptake signal ($S(t)$) was observed. The mice were imaged on their respective GDs of 13, 15 and 17 (term gestation 18–21 days). DCE-MRI imaging volumes were placed at the cervix covering the feto-placental units at the end of the right uterine horn. Additionally, volumes were placed in an orientation that allowed for visualization of the midline sagittal section of the placentas.

Tissue contrast agent concentration vs time (C(t)) maps:

The MRI signal obtained using the spoiled gradient echo sequence from a tissue can be expressed as:

$$S = \frac{S_0\left(1 - e^{-\frac{TR}{T_1}}\right)sin\theta}{1 - cos\theta\, e^{-\frac{TR}{T_1}}} e^{-\frac{TE}{T_2}} \quad (1)$$

where T_1 and T_2 are the tissue longitudinal and transverse

relaxation times respectively. S_o is the effective spin density and θ is the FA. Presence of the contrast agent changes the intrinsic T_1 of the tissue according to the equation:

$$\frac{1}{T_1(t)} = \frac{1}{T_{1,0}} + \alpha_1 C(t) \tag{2}$$

where $C(t)$ is the concentration of the contrast agent in the tissue at any time 't' during the contrast uptake, $T_1(t)$ is the tissue T_1 value at time t, $T_1(t{=}0)$ is the initial baseline T_1 of the tissue and α_1 is the relaxivity (in $(\text{mmol/l})^{-1}$ sec^{-1}) of the injected contrast agent. The α_1 value for Magnevist was taken to be 3.10 ± 0.01 $(\text{mmol/l})^{-1}$ s^{-1} at 7.0 T [39]. The $T_1(t{=}0)$ of the tissue can be obtained using the gradient echo data acquired at three different FAs by fitting it to a linearized form of Eq. (1) [40,41]. The $T_1(t)$ of the tissue at any time t during contrast uptake can be obtained by dividing the signal during contrast uptake by the baseline signal:

$$\frac{S(t)}{S(t=0)} = \frac{\left(1 - e^{-\frac{TR}{T_1(t)}}\right)\cdot\left(1 - cos\theta\, e^{-\frac{TR}{T_1(t=0)}}\right)}{\left(1 - e^{-\frac{TR}{T_1(t=0)}}\right)\cdot\left(1 - cos\theta\, e^{-\frac{TR}{T_1(t)}}\right)} \tag{3}$$

Here $S(t{=}0)$, the baseline tissue signal, was calculated by averaging the signal from the 9 initial time points acquired before the contrast injection.

Simplifying the above expression and assuming $y = \frac{S(t)}{S(t=0)}$ and $x = \frac{\left(1 - cos\theta\, e^{-\frac{TR}{T_1(t=0)}}\right)}{\left(1 - e^{-\frac{TR}{T_1(t=0)}}\right)}$ we obtain,

$$T_1(t) = -\frac{TR}{\ln\left(\frac{x-y}{x-y\cdot cos\theta}\right)} \tag{4}$$

After obtaining the $T_1(t)$ maps from Eq. (4), $C(t)$ maps were calculated using Eq. (2). All the calculations were performed on a pixel by pixel basis to obtain $C(t)$ maps using a custom code written in MATLAB R2010a (MathWorks Inc., Natick, MA, USA).

2.3. Perfusion analysis and measurement of the central canal diameter

Acquired DCE-MRI image volumes were first inspected for the placentas where the midline sagittal plane was visible. To avoid partial voluming effects, perfusion analysis was performed in the single slice corresponding to the placentas' midline sagittal hemisection plane. The midsagittal slice was identified based on the largest cross-section of the placenta observed and the symmetric decrease in the size of the placental cross-section in the preceding and succeeding slices. Based on the contrast uptake curve characteristics, the placental cross-section was segmented into the HPZ and the LPZ using a tissue similarity mapping (TSM) [42,43] algorithm in SPIN (an in-house software of MR Innovations, Inc., Detroit, MI, USA). Once $C(t)$ maps were generated, values from pixels within a compartment at each time point were averaged to obtain the respective mean concentration curves $C_{HPZ}(t)$ and $C_{LPZ}(t)$. The mean concentration, $C_{placenta}(t)$, from the region-of-interest (ROI) containing the whole placental cross-section was also evaluated. These $C_{HPZ}(t)$, $C_{LPZ}(t)$ and $C_{placenta}(t)$ curves were then used to obtain the respective blood perfusion rates. The contrast agent concentration within the fetus was assessed by evaluating signal intensity within an ROI covering the entire fetus.

Perfusion rates were evaluated using the steepest slope method [44]. Steepest slope is a gradient-based approach to quantify perfusion based on the initial uptake phase of the contrast in the target organ [29]. Using this approach, perfusion was quantified from the following relationship [29,44]:

$$F = \frac{\max(C'(t))}{\max(AIF(t))} \tag{5}$$

Here F is the perfusion rate in ml/min/100 ml of the organ, $C'(t)$ is the time-differential of the concentration–time curve and AIF is the arterial input function. We used a reference tissue-based method to estimate AIF with the maternal skeletal muscle tissue as our reference [45,46]. The mean contrast uptake curve for the $C_{muscle}(t)$ was obtained by averaging the signal at each time point from three distinct ROIs placed in the maternal muscle region. To reduce the influence of noise, this $C_{muscle}(t)$ curve was then fitted to an empirical mathematical model (EMM) [47]. The fitted muscle curve, denoted by $\widehat{C}_{muscle}(t)$, was then used to obtain the corresponding AIF(t) curve [48] using the differential equation of the basic Tofts model [16]:

$$AIF(t) = \frac{1}{K_{trans,muscle}}\cdot\frac{d\widehat{C}_{muscle}(t)}{dt} + \frac{\widehat{C}_{muscle}(t)}{v_{e,muscle}} \tag{6}$$

Known values of the volume transfer constant, $K_{trans,muscle}$ of 0.11/min, and the extravascular extracellular tissue space fraction, $v_{e,muscle}$ of 0.2 for the skeletal muscle, were used in Eq. (6) [48]. The peak value of the AIF(t) was then used in Eq. (5) to obtain the perfusion values. Change in perfusion with advancing gestation was statistically evaluated for the three regions, HPZ, LPZ and the ROI containing the whole placental cross-section.

In all placentas included within the DCE-MRI volumes, wherever the CC was clearly visualized, its diameter was systematically measured using the intensity profile drawn across the vessel. The intensity profile across the CC was obtained from a twice-zoomed image. This profile was baseline-corrected and fitted to a Gaussian profile, and the full width at half maximum of this fitted profile was taken as the diameter of the vessel [49].

2.4. Statistical analysis

A single-factor analysis of variance (ANOVA) was performed to test for changes in perfusion and the CC diameter among the three GDs. If the ANOVA test was positive for change, Tukey's post-hoc test was used to identify the gestation pair between which the change was significant. A student's paired t-test was used to evaluate statistical difference in perfusion values of the HPZ and the LPZ regions at a given gestation. A $p < 0.05$ was considered statistically significant.

3. Results

DCE-MRI data was successfully acquired for seven mice. Quantitative perfusion analysis was carried out in 19 placentas at GD13, 20 placentas at GD15 and 14 placentas at GD17. The typical contrast up-take characteristic was observed in all placentas as shown in Fig. 1 [27,29]. Enhancement was initially seen in the CC of the maternal blood space which supplies the HPZ followed by the remaining HPZ. This was followed by relatively slower enhancement of the LPZ. No measurable contrast uptake was observed within the fetus. Also, Fig. 1 shows the segmented regions of the placenta. The average of the normalized concentration–time curves of all placentas at a given gestation for $C_{HPZ}(t)$, $C_{LPZ}(t)$ and $C_{placenta}(t)$ are plotted in Fig. 2. In obtaining these representative average plots, normalization was carried out so as to account for maternal physiologic factors, using the area

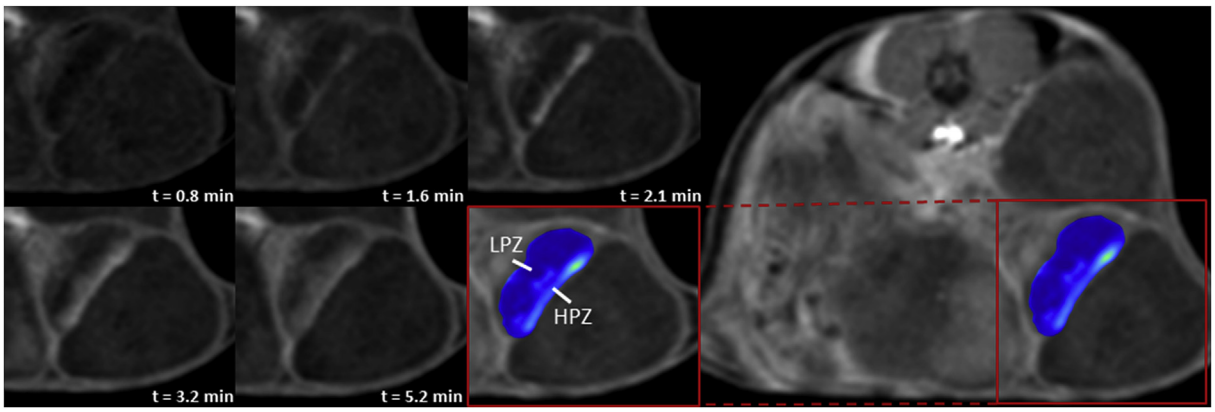

Fig. 1. Contrast-uptake pattern and segmentation of the murine placenta. Temporal contrast uptake characteristic of a murine placenta is shown. Tissue similarity mapping [43] based segmentation of the mouse placenta into the high (light blue) and low perfusion zones (dark blue) at gestational day 15 is also shown.

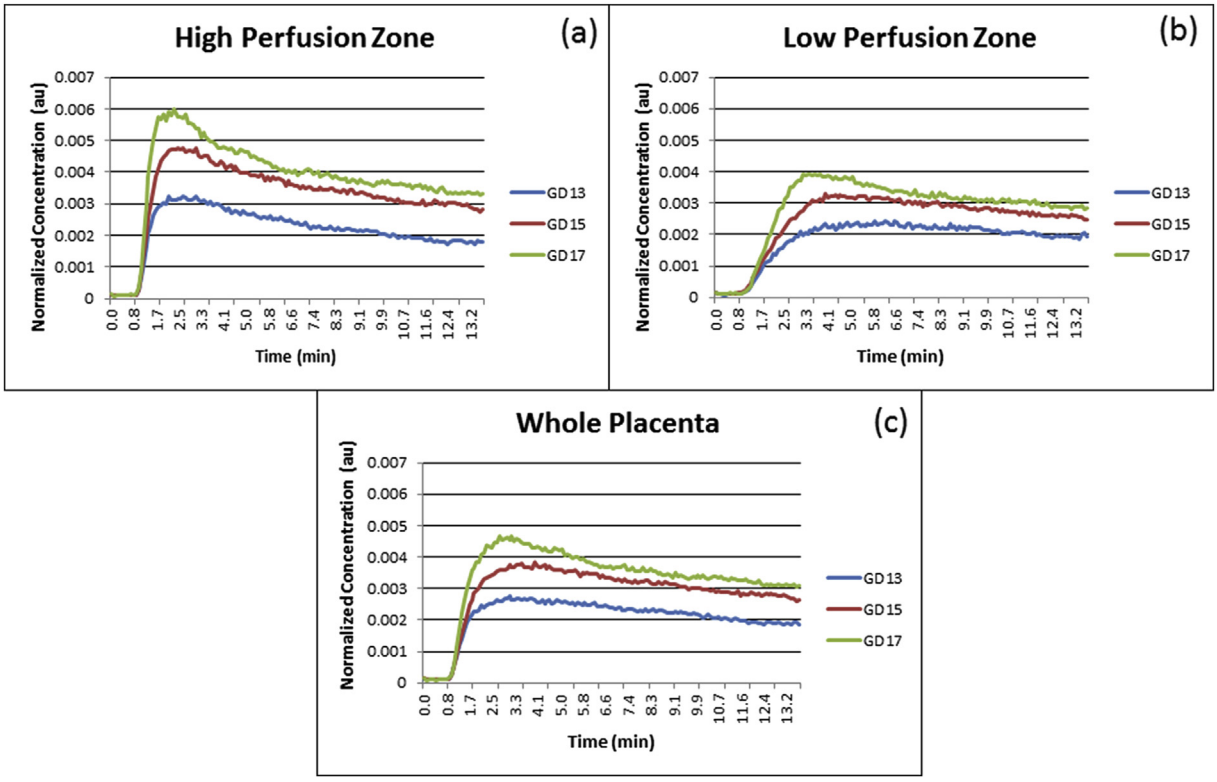

Fig. 2. Placental contrast-uptake curves. Normalized mean concentration–time curves (in arbitrary units (au)) in (A) HPZ, (B) LPZ and (C) the whole placental ROI of normal murine placentas at GDs 13, 15 and 17 are shown. A clear distinction and a significant increase in the mean concentration can be observed across gestational days.

under the curve of the respective maternal skeletal muscle ($C_{muscle}(t)$). A clear distinction was observed between the contrast uptake features of the HPZ, LPZ and the whole placenta between GD13 and GD17. Mean AIF for a given gestation, obtained by taking the average of the AIFs estimated from the fitted $C_{muscle}(t)$ curves for each mouse, is shown in Fig. 3a. Here, too, a clear difference is observed on GD17 relative to GD13. Standard deviation associated with the mean AIF curve at GD13 and GD17 is shown along with that of the corresponding mean $C_{muscle}(t)$ curve in Fig. 3b and c.

Quantitative perfusion results and CC diameter values are plotted in Fig. 4. Measurements of perfusion in the HPZ were as follows: 106.23 ± 56.32, 139.04 ± 55.41 and 172.19 ± 85.57 ml/min/100 ml at GD13, GD15 and GD17 respectively. In the LPZ, the corresponding values were 50.24 ± 31.18, 73.74 ± 39.95 and 75.59 ± 37.56 ml/min/100 ml at GDs 13, 15 and 17 respectively. In the whole placental ROI, perfusion was found to be 61.2 ± 31.2, 90.26 ± 43.67 and 104.94 ± 76.13 ml/min/100 ml at GDs 13, 15 and 17 respectively. As a function of gestation, an increase in perfusion was observed between GD13 and GD17 in the HPZ ($p = 0.02$). In the whole placental ROI as well, perfusion increased significantly between GD13 and GD17 ($p < 0.05$). Perfusion in the LPZ, although showing an increasing trend across the three GDs, the change was not significant ($p = 0.07$). The CC diameter increased significantly ($p < 0.05$) with advancing gestation, with the diameter being 217.4 ± 46 μm, 251 ± 89 μm and 307 ± 61 μm at GD13, GD15 and GD17 respectively.

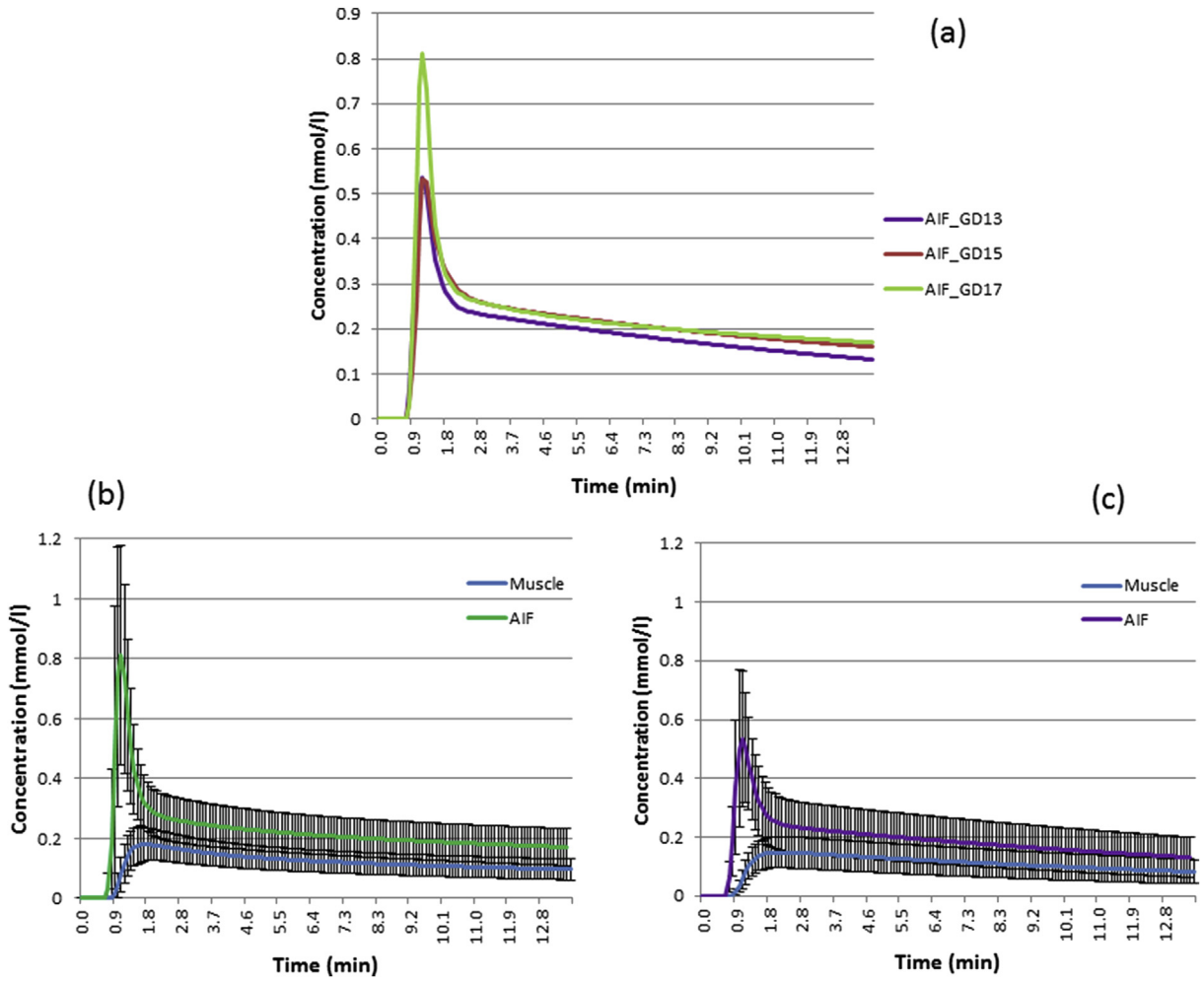

Fig. 3. Quantified AIF concentration-time curves. (a) Mean arterial input function curves (AIFs) for gestational days 13, 15 and 17. Mean AIF here indicates the mean across the 7 mice studied. In (b) and (c) the mean AIF and $C_{muscle}(t)$ curves for gestational days 17 and 13 are plotted respectively along with their associated standard deviations to indicate the extent of the inter-mice variation of the AIF.

4. Discussion

Murine placental perfusion at three different time points in mid and late gestation was measured in a longitudinal cohort of pregnant CD-1 mice using DCE-MRI. Major findings of this study are as follows: (1) a significant increase in placental perfusion was observed between GD13 and GD17; (2) regional differences were observed in gestational age-dependent change in perfusion. While the HPZ showed a significant increase in perfusion between GD13 and GD17, the increase in LPZ perfusion was not significant; and (3) the diameter of the maternal CC increased with advancing gestation.

No contrast uptake was observed in the fetus indicating that the transfer of contrast agent from the maternal side to the fetal side of the placental circulation was not significant during the period of data collection. Hence, our results pertain to the perfusion of the maternal blood space within the placenta. Maternal blood enters the murine placenta through the CC and percolates radially out and down into the tortuous sinusoidal blood space [32]. The CC is supplied by the spiral arteries that, in turn, are supplied by the radial arteries [32]. Between GD13 and GD17, previous Doppler studies reported a relative increase of roughly 70% in the peak blood flow velocity in the CC of the placenta in CD-1 mice [50]. In this context, our results also show a relative perfusion increase of 71% (43.7 ml/min/100 ml) in the whole placental ROI between GD13 and GD17. The observed increase seems to be primarily from the large increase (65.95 ml/min/100 ml between GD13 and GD17) in perfusion to the HPZ that roughly corresponds to the base of the labyrinth zone. Only a small increase of 25.35 ml/min/100 ml was observed in the LPZ between GD13 and GD17. The gestational age-dependent increase in perfusion to the HPZ could be a combined effect of an increase in blood flow velocity and an increase in the size of the CC [32,51]. Our data, in part, support this hypothesis. We found a significant increment in the diameter of the CC between GD13 and GD15 and between GD15 and GD17, driving more and more blood flow into the placenta with advancing gestation [36]. Due to the lack of one-to-one correspondence between the placentas from which perfusion was measured vs. those from which the CC diameter was measured, direct evaluation of the contribution of CC size to the corresponding placental perfusion was not possible. A moderate ($p = 0.09$) correlation, however, is observed between the mean perfusion and the mean CC diameter of the HPZ ($r = 0.98$) as a function of gestation. Further studies are needed to evaluate the relative contributions of the increase in blood flow velocity vs. CC diameter to the overall gestation-dependent increase in placental perfusion.

Late gestation murine placental perfusion values in the literature are in broad agreement with values obtained in our study [27,29]. A recent study measured the regional placental perfusion

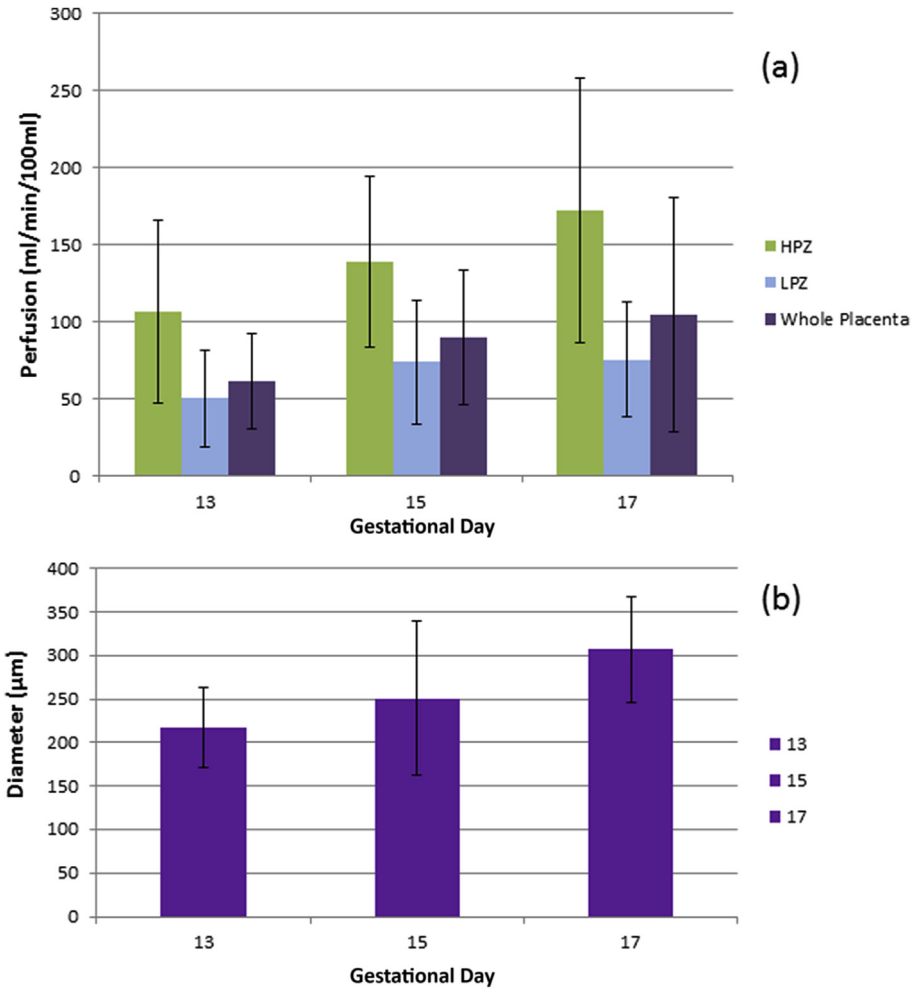

Fig. 4. Murine placental perfusion and central canal diameter values. (a) Blood perfusion (±standard deviation) in the high perfusion zone (HPZ), low perfusion zone (LPZ) and the whole placental ROI at GDs 13, 15 and 17. A trend of increasing perfusion with advancing gestation is seen. Significant increase in perfusion is observed in the HPZ ($p = 0.02$) and the whole placental ROI ($p = 0.04$) between GD13 and GD17. (b) Diameter of the central canal (±standard deviation) at GDs 13, 15 and 17. The diameter increases significantly ($p < 0.05$) between GD13 and GD17.

in late gestation mice at two different days (GDs 14.5 and 16.5) in a cross-sectional cohort of BALB/c mice [29]. However, no significant difference in perfusion was observed. In contrast, we studied placental perfusion starting from midgestation and observed an increase from mid to late gestation. Previous ultrasound studies have shown that there is almost a linear increase in the maternal blood flow velocity to the placenta [35,50] with advancing gestation. Furthermore, a substantial change in maternal blood space morphology occurs between GD12.5 and GD16.5, and after GD16.5 the morphology is relatively unchanged [4]. These features could explain the variation that we observed.

A 2D MR acquisition with a finite slice-gap was used in this study to acquire the DCE-MRI data as it offers higher temporal and in-plane spatial resolution compared to 3D acquisitions. Multiple slices were acquired so as to cover mid-sections of more than one placenta. Due to the presence of the slice gap, however, evaluating perfusion in the entire placental volume was not possible. Hence, we used the single slice corresponding to the mid-sagittal plane of the placenta in our analysis. Because of the typical radial symmetry of the murine placental structure, the results from analyzing the central placental slice are representative of the entire placental volume. It is for similar reasons that the analysis of the central mid-sagittal placental slice is a common practice in histology studies [4] and is also the approach used in other studies of murine placental perfusion [27,28]. The slice containing the placental hemisection/mid-sagittal plane was identified visually based on the criteria of size and symmetry. However, there may be differences from one placenta to the other in the angle that the imaging slice made with the axial plane of the placenta. This could have contributed to the inter-placental differences in the measured perfusion and consequently to the standard deviation of the measured value at a given gestation. Despite this, a significant increase in perfusion was observed from mid to late gestation.

High temporal resolution, on the order of 1 volume per second [52], along with a multi-echo data acquisition scheme to account for T2* effects in the first pass [53], would typically be required for the accurate estimation of AIF. Such high temporal resolution, on the other hand, limits our ability to simultaneously acquire data at high spatial resolution and/or from multiple placentas. We used an acquisition scheme that allowed for slightly lower temporal but higher spatial resolution and coverage. This limited our ability to obtain an AIF through direct measurement. Consequently, we used a reference tissue-based approach to obtain a data-derived arterial input function. Using reference tissue for AIF estimation is a common approach in DCE-MRI and provides reliable results [45,46]. By such an approach, the choice of $K_{trans,muscle}$ and $v_{e,muscle}$ values

influences the AIF curve shape (peak and the steady state value). While there is considerable variability in the literature for these values of skeletal muscle [45,46,48,54,55], we used the recently reported values [48]. These tissue properties for the skeletal muscle are assumed to be the same across the three gestations. Thus, while the choice of the $K_{trans,muscle}$ and $v_{e,muscle}$ values may influence the absolute perfusion values, it does not affect the relative perfusion changes observed in the study. To minimize the influence of noise in the reference tissue curve, we followed the approach suggested by Heisen et al. [56], using EMM to fit the $C_{muscle}(t)$ curve that was then used for the estimation of AIF(t). EMM provided excellent fit for the $C_{muscle}(t)$ curve, where the mean R^2 value for the fit was 0.94 across all curves, with the minimum being 0.84. Additionally, average $C(t)$ curves were used to obtain the perfusion values. This approach does not allow for evaluating more local changes within the ROI, e.g., variations within the HPZ or the LPZ [31]. However, such an approach improves the SNR of the $C(t)$, curve, thus improving the robustness of the measured perfusion parameter for a given compartment/ROI. The amount of contrast agent injected was fixed across the gestations. This leads to a slightly different effective dosage at different gestations. Based on the average weight of the mice at a given gestation, the dosage changed from approximately 0.34 mmol/kg at GD13 to 0.3 mmol/kg at GD17. This actually leads to an underestimation of perfusion at GD17 [57,58] relative to a fixed dosage of 0.34 mmol/kg. Despite this underestimation, we see a significant increase in placental perfusion with advancing gestation. Thus, the small difference in effective dosage at different gestations does not affect the conclusions of the study.

The study was performed on the same set of pregnant mice imaged longitudinally on three GDs. The presence of any remnant contrast within the tissue can alter the baseline T_1 of the tissue. However, since our analysis is based on the temporal rate of contrast uptake, a change in the baseline T_1 of the tissue was not expected to influence our results. Nonetheless, we evaluated the baseline T_1 value of the maternal skeletal muscle tissue in each mouse before the administration of the contrast agent. We found no change in the baseline T_1 ($p = 0.3$), indicating no significant amount of remnant contrast within the mice. During longitudinal scans of the same pregnant mice, identifying the same placenta (s) between different GDs was not possible [59]. Hence, the average data from a group of placentas, at a given gestation, is presented. Nevertheless, this aspect should not affect the conclusions of this study because, despite some placenta-to-placenta variation, significant changes with gestational age were found in the whole placenta as well as in one of its constituent regions. Finally, due to the relatively short duration of the DCE-MRI study post injection (~14 min), we did not see any contrast uptake in the fetus. Future studies focused on evaluating perfusion on the fetal side of the placenta may require longer study durations with the use of appropriate mathematical models for placental exchange [27,28] and/or the use of a different contrast agent that can readily cross the interhemal membrane.

5. Conclusion

In this longitudinal study, using DCE-MRI, we evaluated for the first time the gestational age-dependent perfusion changes in the normal murine placenta and its regional compartments. The constituent placental regions differ in their gestational age-dependent changes of perfusion. Hence, it may be important to focus on regional perfusion changes rather than changes in the overall placental perfusion in future studies of placental pathology. Finally, the diameter of the maternal CC increases by more than 40% between GDs 13 and 17, and could be playing an important role in the increase in placental perfusion with advancing gestation.

Conflicts of interest

The authors have no conflicts of interest.

Acknowledgments

This research was supported, in part, by the Perinatology Research Branch, Division of Intramural Research, *Eunice Kennedy Shriver* National Institute of Child Health and Human Development (NICHD), National Institutes of Health (NIH), Department of Health and Human Services (DHHS); and, in part, with Federal funds from NICHD (NIH, DHHS) under Contract No. HHSN275201300006C. The authors are grateful to Dr. Theodore Price (Perinatology Research Branch), Dr. Lisa J. Brossia-Root, Laura Lee McIntyre, and all personnel involved in the Division of Laboratory Animal Resources (Wayne State University). This work was also supported, in part, by a Small Business Technology Transfer (STTR) grant from the National Heart, Lung, and Blood Institute (NHLBI, NIH, DHHS; 1R42HL112580-01A1), by Wayne State University's Perinatal Research Initiative and by the Perinatology Virtual Discovery Grant to J.N. (made possible by the W.K. Kellogg Foundation award P3018205).

References

[1] C.R. Rosenfeld, Regulation of the placental circulation, in: R.A. Polin, W.W. Fox, S.H. Abman (Eds.), Fetal and Neonatal Physiology, Saunders, Philadelphia, 2004.
[2] P. Kaufmann, T.M. Mayhew, D.S. Charnock-Jones, Aspects of human fetoplacental vasculogenesis and angiogenesis. II. Changes during normal pregnancy, Placenta 25 (2–3) (2004) 114–126.
[3] P. Coan, A. Ferguson-Smith, G. Burton, Ultrastructural changes in the interhaemal membrane and junctional zone of the murine chorioallantoic placenta across gestation, J. Anat. 207 (6) (2005) 783–796.
[4] P.M. Coan, A.C. Ferguson-Smith, G.J. Burton, Developmental dynamics of the definitive mouse placenta assessed by stereology, Biol. Reprod. 70 (6) (2004) 1806–1813.
[5] M.Y. Rennie, et al., Expansion of the fetoplacental vasculature in late gestation is strain dependent in mice, Am. J. Physiol. Heart Circul. Physiol. 302 (6) (2012) H1261–H1273.
[6] M.Y. Rennie, et al., 3D visualisation and quantification by microcomputed tomography of late gestational changes in the arterial and venous feto-placental vasculature of the mouse, Placenta 28 (8–9) (2007) 833–840.
[7] G.J. Burton, D.S. Charnock-Jones, E. Jauniaux, Regulation of vascular growth and function in the human placenta, Reproduction 138 (6) (2009) 895–902.
[8] C.R. Rosenfeld, et al., Circulatory changes in the reproductive tissues of ewes during pregnancy, Gynecol. Invest 5 (5–6) (1974) 252–268.
[9] I.A. Brosens, W.B. Robertson, H.G. Dixon, The role of the spiral arteries in the pathogenesis of preeclampsia, Obstet. Gynecol. Annu. 1 (1972) 177–191.
[10] I. Brosens, H.G. Dixon, W.B. Robertson, Fetal growth retardation and the arteries of the placental bed, Br. J. Obstet. Gynaecol. 84 (9) (1977) 656–663.
[11] J.J. Brosens, R. Pijnenborg, I.A. Brosens, The myometrial junctional zone spiral arteries in normal and abnormal pregnancies: a review of the literature, Am. J. Obstet. Gynecol. 187 (5) (2002) 1416–1423.
[12] S. Yagel, et al., Placental blood flow measured by simultaneous multigate spectral Doppler imaging in pregnancies complicated by placental vascular abnormalities, Ultrasound Obstet. Gynecol. 14 (4) (1999) 262–266.
[13] C.V. Ananth, A.M. Vintzileos, Ischemic placental disease: epidemiology and risk factors, Eur. J. Obstet. Gynecol. Reprod. Biol. 159 (1) (2011) 77–82.
[14] B.J. Trudinger, et al., Fetal umbilical artery flow velocity waveforms and placental resistance: clinical significance, Br. J. Obstet. Gynaecol. 92 (1) (1985) 23–30.
[15] T. Stampalija, G.M. Gyte, Z. Alfirevic, Utero-placental Doppler ultrasound for improving pregnancy outcome, Cochrane Database Syst. Rev. (9) (2010) CD008363.
[16] P.S. Tofts, et al., Estimating kinetic parameters from dynamic contrast-enhanced T(1)-weighted MRI of a diffusable tracer: standardized quantities and symbols, J. Magn. Reson Imaging 10 (3) (1999) 223–232.
[17] Radiology, A.C.o., ACR Manual on Contrast Media, Version 8, 2012, 2011.
[18] T.M. Tomlinson, et al., Magnetic resonance imaging of hypoxic injury to the murine placenta, Am J Physiol Regul Integr Comp Physiol 298 (2) (2010) R312–R319.
[19] M. Alison, et al., Measurement of placental perfusion by dynamic contrast-enhanced MRI at 4.7 T, Invest Radiol. 48 (7) (2013) 535–542.
[20] P. Georgiades, A.C. Ferguson-Smith, G.J. Burton, Comparative developmental anatomy of the murine and human definitive placentae, Placenta 23 (1) (2002) 3–19.

[21] J. Rossant, J.C. Cross, Placental development: lessons from mouse mutants, Nat. Rev. Genet. 2 (7) (2001) 538–548.
[22] E.D. Watson, J.C. Cross, Development of structures and transport functions in the mouse placenta, Physiol. (Bethesda) 20 (2005) 180–193.
[23] M.R. Dilworth, C.P. Sibley, Review: transport across the placenta of mice and women, Placenta (34 Suppl) (2013) S34–S39.
[24] H.L. Cheng, Dynamic contrast-enhanced MRI in oncology drug development, Curr. Clin. Pharmacol. 2 (2) (2007) 111–122.
[25] B.F. Coolen, et al., Contrast-enhanced MRI of murine myocardial infarction - part II, NMR Biomed. 25 (8) (2012) 969–984.
[26] K.C. Chan, M.M. Cheung, E.X. Wu, In vivo multiparametric magnetic resonance imaging and spectroscopy of rodent visual system, J. Integr. Neurosci. 9 (4) (2010) 477–508.
[27] L.J. Salomon, et al., Placental perfusion MR imaging with contrast agents in a mouse model, Radiology 235 (1) (2005) 73–80.
[28] F. Taillieu, et al., Placental perfusion and permeability: simultaneous assessment with dual-echo contrast-enhanced MR imaging in mice, Radiology 241 (3) (2006) 737–745.
[29] C.C. Remus, et al., Application of the steepest slope model reveals different perfusion territories within the mouse placenta, Placenta 34 (10) (2013) 899–906.
[30] L.J. Salomon, et al., In vivo dynamic MRI measurement of the noradrenaline-induced reduction in placental blood flow in mice, Placenta 27 (9–10) (2006) 1007–1013.
[31] E. Solomon, et al., Major mouse placental compartments revealed by diffusion-weighted MRI, contrast-enhanced MRI, and fluorescence imaging, Proc. Natl. Acad. Sci. U. S. A. 111 (28) (2014) 10353–10358.
[32] S.L. Adamson, et al., Interactions between trophoblast cells and the maternal and fetal circulation in the mouse placenta, Dev. Biol. 250 (2) (2002) 358–373.
[33] L.P. Reynolds, et al., Evidence for altered placental blood flow and vascularity in compromised pregnancies, J. Physiol. 572 (Pt 1) (2006) 51–58.
[34] E. Hernandez-Andrade, et al., Evaluation of utero-placental and fetal hemodynamic parameters throughout gestation in pregnant mice using high-frequency ultrasound, Ultrasound Med. Biol. 40 (2) (2014) 351–360.
[35] Y.-J. Zhou, et al., Real-time placental perfusion on contrast-enhanced ultrasound and parametric imaging analysis in rats at different gestation time and different portions of placenta, PloS one 8 (4) (2013) e58986.
[36] C. Arthuis, et al., New insights into uteroplacental perfusion: quantitative analysis using Doppler and contrast-enhanced ultrasound imaging, Placenta 34 (5) (2013) 424–431.
[37] F. Kording, et al., Automatic differentiation of placental perfusion compartments by time-to-peak analysis in mice, Placenta 36 (3) (2015) 255–261.
[38] Guide for the Care and Use of Laboratory Animals: Eighth Edition, The National Academies Press, 2011.
[39] C. Kalavagunta, G. Metzger, A field comparison of r1 and r2* relaxivities of Gd-DTPA in aqueous solution and whole blood: 3T versus 7T, Proc. Int. Soc. Magn. Reson. Med. 18 (2010) 4990.
[40] K.A. Christensen, et al., Optimal determination of relaxation times of Fourier transform nuclear magnetic resonance. determination of spin-lattice relaxation times in chemically polarized species, J. Phys. Chem. 78 (19) (1974) 1971–1977.
[41] H.Z. Wang, S.J. Riederer, J.N. Lee, Optimizing the precision in T1 relaxation estimation using limited flip angles, Magnetic Reson. Med. 5 (5) (1987) 399–416.
[42] B.K. Yadav, U. Krishnamurthy, Y. Shen, J. Neelavalli, G. Szalai, B. Wang, T. Chaiworapongsa, E. Hernandez-Andrade, N.G. Than, E.M. Haacke, R. Romero, Evaluating placental growth in normal murine pregnancy using tissue-similarity-mapping and dynamic contrast enhanced magnetic resonance imaging, in: Joint Annual Meeting ISMRM-ESMRMB 2014, 2014. Milan, Italy.
[43] E.M. Haacke, M. Li, F. Juvvigunta, Tissue similarity maps (TSMs): a new means of mapping vascular behavior and calculating relative blood volume in perfusion weighted imaging, Magn. Reson Imaging 31 (4) (2013) 481–489.
[44] K.A. Miles, Measurement of tissue perfusion by dynamic computed tomography, Br. J. Radiol. 64 (761) (1991) 409–412.
[45] D.A. Kovar, M. Lewis, G.S. Karczmar, A new method for imaging perfusion and contrast extraction fraction: input functions derived from reference tissues, J. Magn. Reson Imaging 8 (5) (1998) 1126–1134.
[46] T.E. Yankeelov, et al., Quantitative pharmacokinetic analysis of DCE-MRI data without an arterial input function: a reference region model, Magn. Reson Imaging 23 (4) (2005) 519–529.
[47] X. Fan, et al., New model for analysis of dynamic contrast-enhanced MRI data distinguishes metastatic from nonmetastatic transplanted rodent prostate tumors, Magn. Reson Med. 51 (3) (2004) 487–494.
[48] M. Heisen, et al., The use of a reference tissue arterial input function with low-temporal-resolution DCE-MRI data, Phys. Med. Biol. 55 (16) (2010) 4871–4883.
[49] L. Zhou, et al., The detection and quantification of retinopathy using digital angiograms. medical imaging, IEEE Trans. 13 (4) (1994) 619–626.
[50] J. Mu, S.L. Adamson, Developmental changes in hemodynamics of uterine artery, utero- and umbilicoplacental, and vitelline circulations in mouse throughout gestation, Am J Physiol Heart Circ Physiol 291 (3) (2006) H1421–H1428.
[51] S. Kulandavelu, et al., Endothelial nitric oxide synthase deficiency reduces uterine blood flow, spiral artery elongation, and placental oxygenation in pregnant mice, Hypertension 60 (1) (2012) 231–238.
[52] E. Henderson, B.K. Rutt, T.Y. Lee, Temporal sampling requirements for the tracer kinetics modeling of breast disease, Magn. Reson Imaging 16 (9) (1998) 1057–1073.
[53] H. Uematsu, et al., Vascular permeability: quantitative measurement with double-echo dynamic MR imaging–theory and clinical application, Radiology 214 (3) (2000) 912–917.
[54] T.E. Yankeelov, et al., Repeatability of a reference region model for analysis of murine DCE-MRI data at 7T, J. Magn. Reson Imaging 24 (5) (2006) 1140–1147.
[55] K.M. Donahue, et al., Dynamic Gd-DTPA enhanced MRI measurement of tissue cell volume fraction, Magn. Reson Med. 34 (3) (1995) 423–432.
[56] M. Heisen, et al., The use of a reference tissue arterial input function with low-temporal-resolution DCE-MRI data, Phys. Med. Biol. 55 (16) (2010) 4871–4883.
[57] H. Kostler, et al., Prebolus quantitative MR heart perfusion imaging, Magn. Reson Med. 52 (2) (2004) 296–299.
[58] K. Nikolaou, et al., Quantification of pulmonary blood flow and volume in healthy volunteers by dynamic contrast-enhanced magnetic resonance imaging using a parallel imaging technique, Invest Radiol. 39 (9) (2004) 537–545.
[59] R. Avni, et al., Unique in utero identification of fetuses in multifetal mouse pregnancies by placental bidirectional arterial spin labeling MRI, Magn. Reson Med. 68 (2) (2012) 560–570.